LAUTECH Journal of Engineering and Technology 19 (2) 2025: 52-63

10.36108/laujet/5202.91.0260

Mechanical and Structural Impacts of Fly-ash Reinforcement on Graphite-Aluminum Composites

[1*]Enwerem G. C, [2]Asafa T. B, and [3]Durowoju M. O.

[1] Mechanical Engineering Department, Federal Polytechnic, Ede, Osun State, Nigeria,
[2,3]Mechanical Engineering Department, Ladoke Akintola University of Technology, Ogbomoso, Oyo State, Nigeria.

Article Info

Article history:

Received: Feb 20, 2025
Revised: Mar 16, 2025
Accepted: Mar 27, 2025

Keywords:

Aluminum,
Composite,
Fly-ash,
Graphite,
Reinforcement

Corresponding Author:
chuks16a@gmail.com

ABSTRACT

Materials with light-weight, optimum thermo-mechanical properties are in great demands for thermal management systems. Graphite-Aluminum (Gr-Al) composites are being reinforced to achieve the above objectives. This paper reports the effects of fly-ash powder on the mechanical and structural characteristics of spark plasma-sintered Gr-Al composites. Graphite powder (53 µm) and 20%wt aluminum powder (1-2 µm), were reinforced with 0, 10, 20, and 30 %wt fly-ash powder (53 µm), designated as GA, GAF-1, GAF-2 and GAF-3, respectively. Sintering was conducted at a heating rate of 50 oC/min, temperature of 550 oC, pressure of 5x10-2 mbar and 10-minute holding time. Characterization was based on morphology, microhardness, displacement, relative density, peak intensity ratios and tensile strength. The fly-ash particles had cup-like shape with dominance clearly noticeable in GAF-3. GAF-1 had the highest increase in peak intensity of 12.67%. GA showed the highest displacement rate (0.983 mm/mins within the first 4 minutes of heating), and instantaneous relative density (0.97). However, increase in fly-ash led to 11.22% increase in porosity and 35.85% increase in the micro-hardness while GAF-3 gave the highest ultimate tensile strength of 388.92 MPa. Reinforcing Gr-Al matrix with Fly-ash makes it suitable for industrial applications.

INTRODUCTION

The continuous demands for lightweight materials for diverse engineering applications have led to research into graphite-aluminum composite developments. Graphite (a grey crystalline allotropic form of carbon) also has a high melting temperature, low coefficient of thermal expansion, and self-lubricating property (Rodriguez *et al.*, 2006). Graphite can be produced through the pyrolysis of biomass (Li *et al.*, 2014) and finds application in a wide range of areas like thermal management systems (Klet and Conway, 2000; McCoy and Vrable, 2004), electronics industry, battery anodes, die materials in sintering furnaces (Asafa *et al.*, 2015) and solid lubricant in pencils. Graphite has a problem of brittleness, which makes its consolidation difficult, hence the need for binders like Copper, Silver, and Aluminum among others (Fukushima, 2009; Durowoju 2016).

Graphite-aluminum interface has the problem of wettability, hence the need for a wetting agent. Studies have also shown that ensuring the wettability of graphite particles using low melting point metals and materials like Lead, Silicon dioxide, and Aluminum as wetting agents, could also lead to reduced porosity (Karoly *et al.*, 2014; Olatinwo et al., 2024). Several materials have been used in literature for the reinforcement of composites. Prominent among the reinforcement materials used on Aluminum materials include but are not limited to SiO_2, SiC, Si, Cu, and Mg (Subramani *et al.*, 2013; Govindarao *et al.*, 2017). Other materials used for reinforcement in composites include snail shell powder (Asafa *et al.*,

2015), carbon fiber, diamond, carbon nanotubes, and graphene (Huang *et al*., 2014).

Fly ash is a fine powdery substance that flies up from coal combustion chambers (boilers) captured by emission control facilities such as electrostatic precipitators or fabric filters and scrubbers installed in the chambers and they are considered waste. Türkel and Aksin (2012) stated that over 15 million tons of fly ash (FA) are produced in Turkey every year as by-products of industrial production. The chemical, mineralogical, and physical properties of fly ash can vary significantly from one source to another based on the differences in fuel sources (coal), combustion conditions, and cooling regimes (Karla *et al*., 2012). Fly-ash finds application as raw material and substitute in brick or concrete productions and construction purposes (Türkel and Aksin, 2012; Yazici and Arel, 2012; Kelechi *et al.*, 2022), and it is also used as a component in road bases, sub-bases and pavements (Dwivedi and Jain, 2014). In this work, we reinforced the Gr-Al composite with fly ash particles. The need here is for a composite material replacement for the aluminum alloy to reduce weight and increase fuel efficiency while ensuring mechanical stability and environmental preservation (Grabias-Blicharz and Franus, 2023). Few researches (Arasukumar *et al*., 2012; Zhou *et al*., 2014) have shown that graphite gives better weight reduction over aluminum materials and provides better thermal stability at higher temperature ranges than aluminum. This justifies the reason for making graphite produced from wastes as the base material (matrix) as against the conventional Aluminum metal matrix composite (AMMC) as found in previous studies in which fractions of Gr such as 0-4 wt% (Saheb, 2011; Rajesh *et al*., 2017), 3-4 wt% (Selvan and Sivaram, 2017) and 3 wt% (Viswanatha *et al*., 2013) were utilized. Attempts at using graphite powder as the matrix material in the fabrication of composite materials with comparable and competitive qualities for automotive, sports, defense, and aerospace applications are yet to be fully explored. Therefore, this study is designed to examine the effects of the variation of fly ash on the mechanical and structural properties of the spark plasma sintered graphite-aluminum composite.

MATERIALS AND METHODS

One thousand pieces of discarded 1.5 V dry cell batteries were collected around Ede, Osun State, Southwest, Nigeria, sorted and sectioned to remove the inner rods. The rods were then washed with distilled water, dried, and pulverized in the XQ-2B Inlay Pulverizing machine for 15 hours to obtain graphite particles of 53 µm average size using standard sieves. Aluminum powder of 1-2 µm size (99.8% purity) was purchased from F. J. Broadman and Co. at Haney, United States. The fly ash was obtained from the Ekson power plant in South Africa and sieved using standard sieves with 53 µm sieve size. The initial powders were combined based on the compositions specified in Table 1 with aluminum kept at 20 wt% for all samples. The experimental setup contained four composite samples based on the existing standard volume ratio range of between 60/40 and 95/5 % for graphite to metal reinforcement in the composite (Fukushima, 2009). The powders were thoroughly mixed using a T2F Tubular mixer having a tungsten carbide ball with a ball-to-powder ratio of 5:2 at a speed of 101 rpm for one hour. The mixtures were then introduced into the spark plasma sintering (SPS) machine (8604 HHPD25) and sintered at a temperature of 550 ^{o}C, a heating rate of 50 ^{o}C/min, a dwell time of 10 mins, and furnace pressure of 1 mbar. A compressive load of 10 kN with a uniaxial pressure of 50 MPa was applied in between the graphite punches during sintering. The pyrometer attached to the top of the die at 5 mm from the surface was utilized to

measure the temperature of the samples while the linear shrinkage of the powder compact was measured as displacement and displacement rate in response to the relative displacement of the graphite punch. Discs of 20 mm in diameter of the sintered powders were then produced for each of the samples.

Table 1: Composition of the fabricated composites used in this study

Coded Name	**Composition (wt%)**		
	Gr	**Al**	**Fly-Ash**
GA	80	20	0
GAF-1	70	20	10
GAF-2	60	20	20
GAF-3	50	20	30

The initial powders and the sintered samples were characterized using X-ray diffraction (XRD, D8 advanced X-Ray diffractometer) and Scanning Electron Microscopy (SEM, Phenom ProX made by Phenomworld Eindhoven Netherlands) techniques. XRD scan was performed at operating conditions of 40 kV/40 mA utilizing Cu Kα radiation (λ = 0.15406 nm) at a scanning speed of 5 ^{o}/min within a range of diffraction angle of 20^{o} - 70^{o}. The diffraction patterns from the samples were processed with X'Pert High Score Plus software. The crystal size D relates to the peak broadening in a diffraction pattern, based on Scherrer's shown in Equation 1 (Frischa *et al*., 2014; Wu *et al*., 2017)

$$D = \frac{k\lambda}{\beta cos\theta} \quad (1)$$

Where k is the shape factor, λ is the wavelength of the X-rays, β is the full-width-at-half maximum intensity, and θ is the Bragg angle. The Peak Intensity Ratio (PIR) defines the ratio of the peak intensity of the second highest to the first highest peak intensity of the metal portion in the sintered samples given as Equation 2 (Selvan and Sivaram, 2017).

$$PIR = \frac{Intensity\ of\ 2^{nd}\ highest\ metallic\ peak}{Intensity\ of\ highest\ metallic\ peak} x\ 100\% \quad (2)$$

The peak intensities were obtained from XRD diffractographs of the samples. The density (ρ_a) of the sintered composite sample was obtained based on Archimedes Principle using BP210S balance (Sartorious AG, Goettingen, Germany) while the theoretical density ρ_C was obtained from Equation 3 (Priyadarshi and Sandhyarani, 2014).

$$\rho_C = (\left(\frac{W_{Gr}}{\rho_{Gr}}\right) + \left(\frac{W_{Fa}}{\rho_{Fa}}\right) + \left(\frac{W_{Al}}{\rho_{Al}}\right))^{-1} \quad (3)$$

Where $\rho_{Fa}, \rho_{Gr},$ and ρ_{Al} are the theoretical densities of fly ash, graphite, and aluminum, respectively; and W_{Fa}, W_{Gr}, and W_{Al} being the weights of fly ash, graphite, and aluminum respectively. The Relative Density (R.D.) of the composite was obtained from Equation 4

$$R.D = \frac{\rho a}{\rho c} * 100\% \quad (4)$$

where ρ_a and ρ_c are the actual and theoretical density, respectively. The porosity P was calculated from Equation 5

$$P = 1 - R.D \quad (5)$$

The volume fraction percentage of voids (V_v) was estimated from Equation 6 (Priyadarshi and Sandhyarani, 2014).

$$V_v = \frac{\rho_C - \rho_a}{\rho_C} \quad (6)$$

The instantaneous relative density (D_i) was obtained from Equation 7 by Durowoju *et al.*, (2016)

$$D_i = D_f \left(\frac{h_f}{h_i}\right) \quad (7)$$

where D_f *is* the final relative density of the sample obtained by the use of Archimedes' principle, h_f and h_i are the final and instantaneous heights of the samples, respectively. The measured density was reported as the arithmetic mean of three different measurements taken for each sample.

Vickers' indentation method was adopted for measuring the micro-hardness of the samples at a load of 100 gf and a dwell time of 15 s. The arithmetic mean of three successive indentations was reported. The yield strength (YS) and the ultimate tensile strength (UTS) were obtained from Equations 8 and 9 as presented in Hashemi, (2011)

$$YS = 2HV + 105 \quad (8)$$

$$UTS = 1.3HV + 344 \quad (9)$$

The yield strength (Y.S) and the tensile strength give an understanding of the probable behavior of these samples under tensile load, and the materials' resistance to indentation.

RESULTS AND DISCUSSION

Morphology of the initial powders and sintered samples

The microstructures of the starting powders are shown in Figure 1. The graphite particles (Figure 1a) have a flake-like morphology, with few nodular particles, while the fly-ash particles (Figure 1b) are oval or ellipsoidal. The aluminum particles are largely irregular in shape as shown in Figure 1c.

Figure 2a shows the microstructure for the sintered sample without fly-ash reinforcement (GA), while Figures 2b, c, and d represent that of the sintered samples with 10, 20, and 30% fly-ash compositions, respectively. From the micrographs, the presence of pores could be noticed, which appeared to be on the increase as the fly-ash content was increased. At GAF-3 (Figure 2d), the oval fly-ash particles appear cup-like after the sintering, which might be due to the increased resistance to compression offered by the SO_2 content in fly-ash.

Phase analysis of the initial powders and the sintered samples

XRD diffractogram of the starting graphite particles showed a dominant presence of carbon (Figure 3a) while aluminum is predominant in the aluminum powder with traces of MnO as an impurity (Figure 3b).

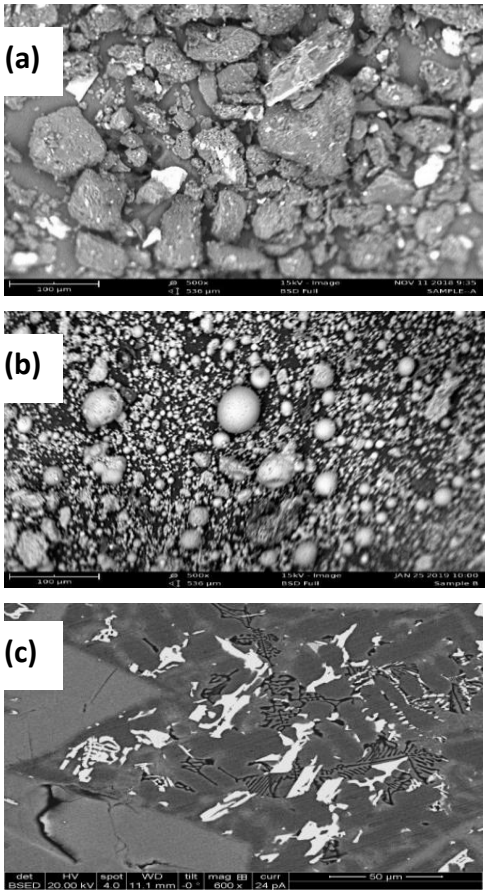

Figure 1: SEM Micrographs of (a) graphite (b) fly-ash (c) aluminum powder

The traces for Gr (in the form of carbon) are observed at 2θ of 27°, 45˚ and 55˚ with respective d-spacing of 3.35 Å, 2.76 Å and 1.7 Å, respectively. For Al particles, peaks are observed at 2θ of 38°, 42°, 65°, 78° and 82° with inter-planar spacing of 2.34 Å and 0.01 Å at 2θ of 65° and 78°, respectively. The fly ash contains majorly silicon dioxide (SiO_2), calcium dioxide (CaO), and aluminum dioxide (Al_2O_3) as shown in Figure 2c,

with percentage fractions of 51.43, 6.75, and 30.93 wt%, respectively, while other components are in minute quantities as shown in Table 2 (Rycroft, 2017).

These results confirm that each of the initial powders (graphite and aluminum) exists in single phases with minimal impurities. The XRD spectra for the phases and compounds present in the initial powders and sintered samples are presented in Figure 3 and Figure 4 respectively.

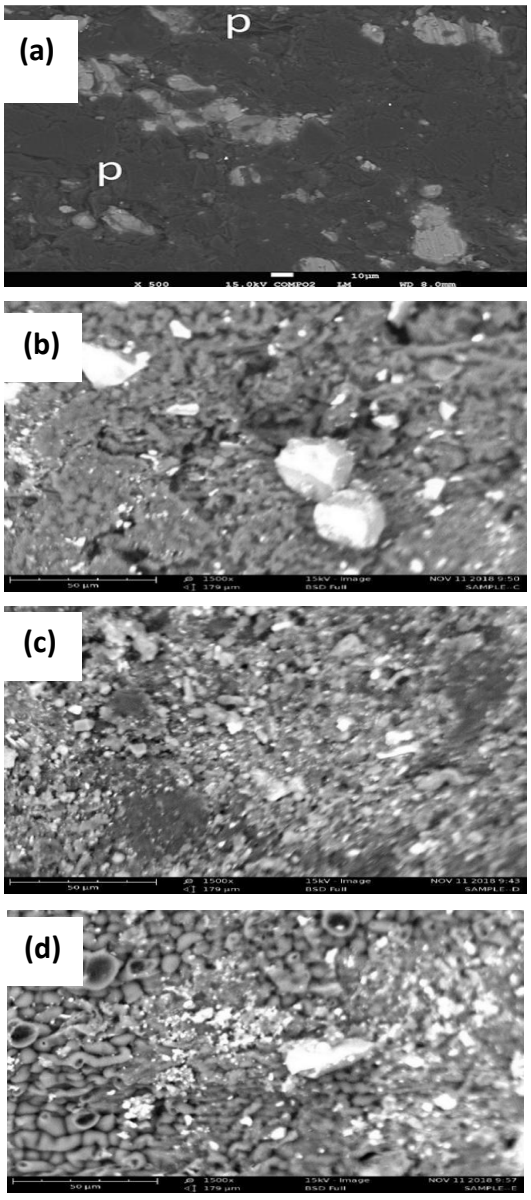

Figure 2: SEM images of (a) GA (b) GAF-1 (c) GAF-2 and (d) GAF-3

More phases and compounds that appear as fly ash were added to the Gr-Al powders (Figure 4b-d). The peaks due to the presence of Gr and Al are enhanced with the addition of fly-ash reinforcement as seen from the intensity values. From Figure 4(b-d), Ca, Si_2C_3 CaC_2, $Al_{12}Mg_{17}$, and Mg_2Al_{12} were observed in either GAF-1, GAF-2, or GAF-3 and they all came from the reactions of fly-ash with Gr (as C), Si and Al during sintering. While magnesium aluminum (Mg_2Al_3) compound with hexagonal packed structure was formed in the GAF-1 sample, GAF-2 and GAF-3 show the presence of aluminum magnesium ($Al_{12}Mg_{17}$) alloy of cubic crystal structure.

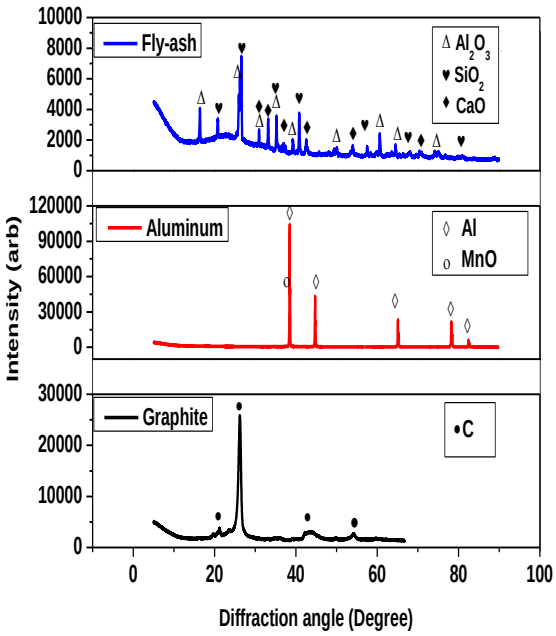

Figure 3: XRD plots for initial (a) graphite (b) aluminum (c) fly-ash powder

Crystal structures have an atomic packing factor of 74% leaving 26% interstitial spaces to be filled. The formation of silicon is due to the possible decomposition of silicon dioxide contained in the fly ash or used as a wetting agent.

Table 2: Compositions of fly ash (Rycroft, 2017).

Components	**Silica (SiO_2)**	**Alumina (Al_2O_3)**	**Calcium Oxide (CaO)**	**Iron Oxide (Fe_2O_3)**	**Others**
Weight (wt%)	51.43	30.93	6.75	2.29	8.60

Peak intensity ratio

The peak intensities and their corresponding intensity ratios as derived from the XRD spectra (Figure 4) are presented in Table 3. The highest value of peak intensity ratio of 86.52% was observed for GAF-1 (sample with 10% fly-ash content).

Table 3: Peak intensity ratio for the sintered samples

Sintered Sample	Highest Peak Intensity (counts)	Second Highest Peak Intensity (counts)	Peak Intensity Ratio (%)
GA	180.971	133.644	73.85
GAF-1	1664.17	1439.92	86.52
GAF-2	3485.22	2304.85	66.13
GAF-3	3092.25	2063.57	66.73

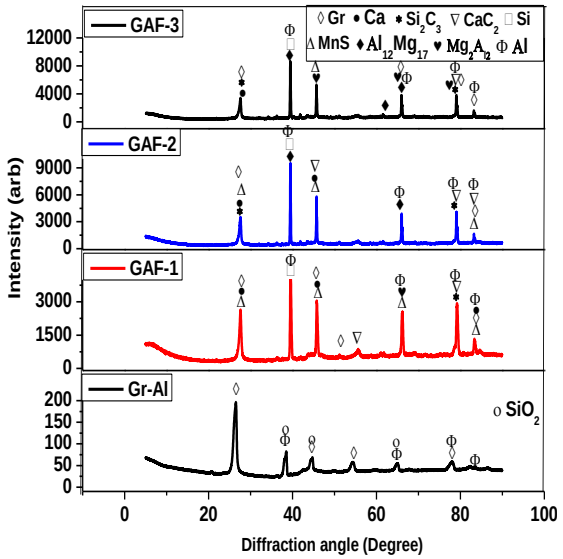

Figure 4. XRD plots for the sintered samples (a) GA and (b) GAF-1 (c) GAF-2 and (d) GAF-3

Displacement and displacement rates

The influence of fly ash as a reinforcement on the displacement and displacement rates of the sintered composite samples is shown in Figure 5. It was observed that the displacements of fly-ash reinforced composites were about three times lower than that of the unreinforced Gr-Al composite (Figure 5a), hence the reason for the high densification of the reinforced samples. However, the differences in displacement values among the reinforced composites were insignificant.

That was justified by the difficulty encountered while compressing ceramic materials (Durowoju *et al*., 2019). At the heating rate of 50 ^{o}C/min, densification started in the Gr-Al sample after about 6 mins of heating compared to that of the reinforced samples where densification started after 11 mins. The presence of fly ash in the composites must have been responsible for the slight variation in their densification behavior. Furthermore, we noticed a sharp compression between 22 and 24 mins followed by expansion for Gr-Al while reinforced composites experienced stepwise compression at around 27th minutes. The unreinforced composite showed four stages of compression/expansion after 5 minutes of sintering compared to three stages in reinforced Gr-Al composites. The temperature variation with time is similar for all the samples as shown in Figure 5b, which indicates that the sintering took place at 550 ^{o}C, while heating and cooling rates were maintained at 50 ^{o}C/min with the dwell time limited to 10 mins. The displacement rate against time for the four samples is presented in Figure 5c. The highest displacement rates of 0.983, 0.436, 0.392, and 0.346 mm/min were obtained from GA, GAF-1, GAF-2, and GAF-3, respectively after about 4 mins of heating.

These results indicate displacement rate decreased with increased fraction of fly-ash content in the Gr-Al composite as observed elsewhere (Durowoju et al., 2016).

For Gr-Al (Figure 5c), four peaks were observed during densification which indicate periods of particle rearrangement, localized and bulk deformation, and extensive sintering. These results are similar to the report of Diouf and Molinari

(2012). However, three peaks were identified for the reinforced samples such that the particle rearrangement and localized deformation stages took place simultaneously (Durowoju, *et al*., 2015; Durowoju, *et al*., 2016) as shown in (Figure 5c, and d).

The displacement behavior at about the 24th minute of sintering (Figure 5a) becomes obvious in the enlarged displacement rate curves (Figure 5d). While the displacement rate for the unreinforced composite is negative, those of the reinforced samples were positive. The positive sign indicates compression while the negative sign connotes expansion. The sudden compression of the Gr-Al between 22 and 24 mins of sintering was seen as a peak in the displacement rate curve. The stepwise compression observed in the reinforced composites at around 27th minutes is considered another step in the displacement rate curves as shown in Figure 5d.

Instantaneous relative density

Reinforcing a composite material with particles like SiO_2, Si, SiC, and fly-ash affect the densification of the composites and invariably the structural properties are also affected in the process (Asafa *et al*, 2020; Durowoju *et al*., 2019; Priyadarshi and Sandhyarani, 2014; Viswanatha *et al*, 2013; Yazici and Arel, 2012).

Figure 6 shows the relationship between the temperature variations and the instantaneous relative densities during the sintering processes for the samples. The graphs represent both the heating and the cooling regimes. The GA sample (with fly-ash content of 0%) showed very distinct and highest instantaneous relative density of about 0.97, with the cooling side ending at instantaneous relative density of 0.95 at 250 ^{o}C.

The three samples with fly ash contents showed similar characteristics before 0.9 instantaneous relative density. This is due to the effects of the SiO_2 content of fly-ash, which makes for a level of difficulty in compressing hard ceramic materials which SiO_2 represents. Similar results were published elsewhere in Mikulionok, 2024; Asafa *et al*, 2020 and Durowoju *et al*., 2019. GAF-1 showed the least instantaneous relative density. Figure 7 summarizes the maximum displacement, maximum displacement rate, and maximum instantaneous relative density for the sintered samples. GA has the highest maximum displacement of about 2.36 mm while GAF-2 has the lowest value of 1.01 mm. The graphs also show that the higher the fly-ash content, the lower the instantaneous relative density of the G-Al composite reinforced with fly-ash powder.

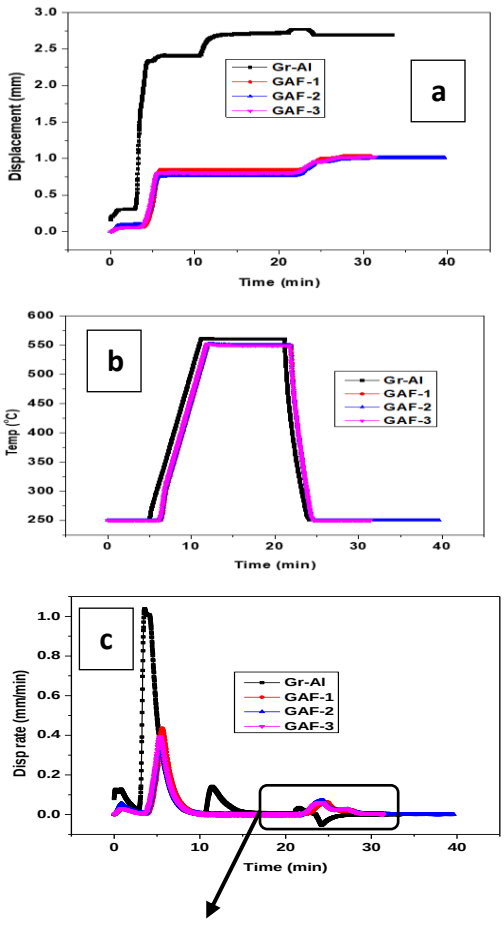

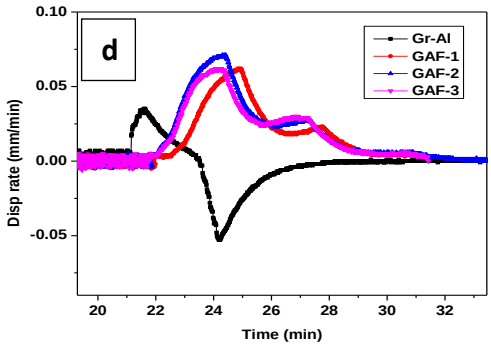

Figure 5: (a) Displacement-time (b) temperature-time(c) displacement rate-time (d) enlarged portion of the displacement rate-time curves.

Density and porosity of the sintered samples

The density and porosity of the sintered samples are shown in Figure 8. The figure results show that the addition of 10 wt% fly-ash to the unreinforced Gr-Al significantly reduced the actual density of 2.3 g/cm^3 by 11% (Figure 8a), reduced the relative density of 97.14% by 8% while increasing the porosity from 2.86% to 10.78% (an increase of 277% as shown in Figure 8b). Within 10 - 30 wt% fly ash content, these properties are insignificantly influenced. For instance, the actual density increased by 1%, relative density decreased by 0.1% while porosity increased by 0.64% when the fly ash content was increased from 10 to 20%.

An increase in porosity might be due to the non-uniform rearrangement of powder particles within the composite when the particles of the fly ash came in between the graphite particles to resist crack initiation. Since both the graphite and fly ash particles were of the same size (53 µm), it becomes easy for pores to exist in between them. This is in line with a previous study by Kane *et al*., (2011), which showed that graphite in its virgin state has a porosity of up to 21.49%.

Micro-hardness and tensile strengths of the sintered samples

The variation of micro-hardness, ultimate tensile strength, and yield strength for the Gr-Al and reinforced samples are presented in Figure 9.

Variations in the values of the micro-hardness of the samples are a reflection of the densification and homogeneity levels of the compaction processes.

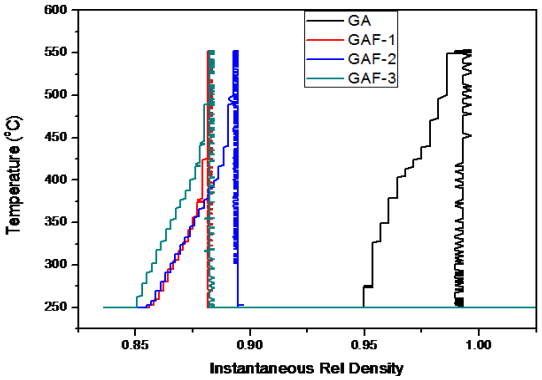

Figure 6. Temperature plots against Instantaneous

The results indicate that the addition of 10 wt% fly ash reduces the micro-hardness of the samples a reflection of the densification and homogeneity levels of the compaction processes. The results indicate that the addition of 10 wt% fly ash reduces the micro-hardness of the Gr-Al composite from 26.85 HV to 25.43 HV. However, the addition of 20 and 30 wt% fly ash enhanced the micro-hardness by 10 and 29%, respectively, compared to the unreinforced Gr-Al.

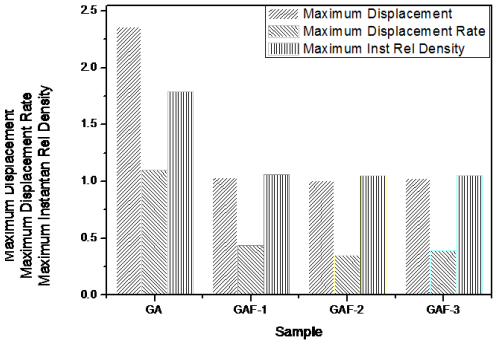

Figure 7. Plots of Maximum Displacement, Maximum Displacement Rate, and Maximum Instantaneous Relative Density against the sintered sample types.

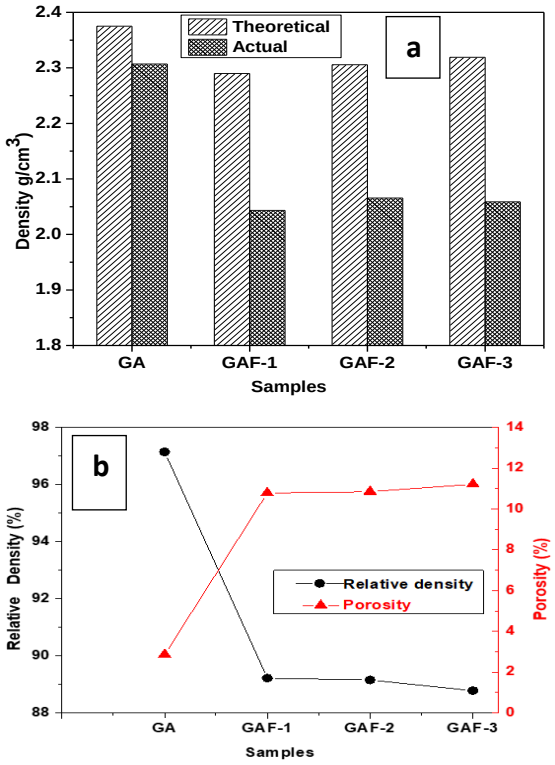

Figure 8: (a) Density (b) Relative density, (c) Porosity of the selected samples

These results show that the fly ash acted as a barrier to the movement of dislocations leading to increased hardness. Silica, being a major composition in fly ash (51.43 wt%) is known for its hardness. Therefore, an increase in fly-ash content invariably meant a direct increase in the ceramic contents of the composites, and also an increase in dislocation density at the particles-matrix interface as shown in Subramani et al. (2013), and subsequently its micro-hardness (Figure 9a). This implies that the reinforced sintered samples will be lighter in weight and also harder than GA (the unreinforced sample).

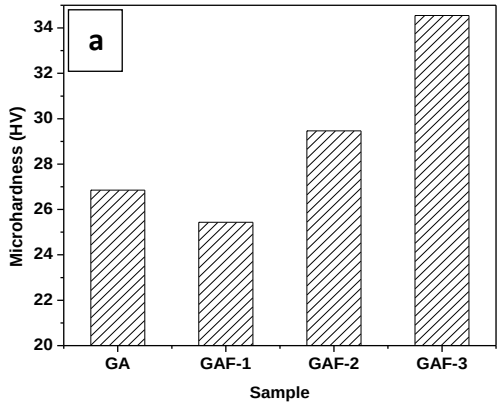

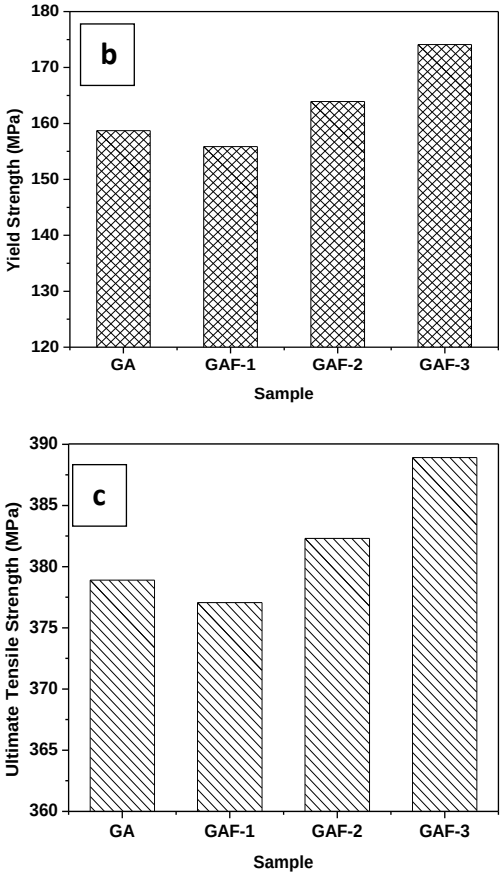

Figure 9: (a) Micro-hardness, (b) Ultimate tensile strength, and (c) Yield strength of the sintered samples

The ultimate tensile strength increased from 377.06 (for GAF-1) to 382.3 MPa (for GAF-2) and finally to 388.92 MPa (for GAF-3) which implies a 2.64% increase over the value for GA (Figure 9b). In the case of the yield strength (Figure 9c), a decrease of 0.49% was observed from 0 to 10% and thereafter the values increased from 155.87 MPa (for GAF-1) to 163.93 (GAF-2, given an increase of 5.17% over GA). The yield strength finally increased to 174.10 MPa (for GAF-3). The increased ultimate tensile strength shows the possible enhancement of the load-carrying capacity which must be due to the load-sharing capability between the matrix and the reinforcement.

The overall effects of the increase in fly-ash content showed an increase in porosity, the highest being at 30% fly-ash reinforcement. A 17.25%

increase in micro-hardness was achieved at 30% fly-ash reinforcement indicating that the higher the fly-ash reinforcement, the higher the hardness of the composite. It could be concluded from the results that the increase in the fly ash of the sintered composite produced a lighter but harder composite material suitable for light vehicle part manufacturing. The reinforcement of Graphite-Aluminum composite with fly-ash powder produced an increase in hardness, porosity, peak intensity (at 10% fly-ash content), ultimate tensile strength, and yield strength.

CONCLUSION

The effects of 10, 20 and 30% addition of fly-ash content on the densification, hardness, peak intensity ratio, ultimate tensile strength, yield strength, and displacement rate of Gr-Al composite have been studied. The Al content was kept constant at 20% in all samples sintered at 550 ^{o}C in an SPS machine. The highest peak intensity of 86.52 % was recorded at a fly ash content of 10 %. The density reduced from 2.307 to 2.0433 g/cm^3 and later exhibited some increase at 20% fly ash content.

REFERENCES

Asafa T.B., Durowoju M.O., Madingwaneng K.P., Diouf S., Sadiku E.R., and Shongwe M.B. (2020). Gr-Al composite reinforced with Si_3N_4 and SiC particles for enhanced micro-hardness and reduced thermal expansion. *Springer Nature*. 2(1026), 1–12.

Asafa T.B., Durowoju M.O., Oyewole A.A., Solomon S.O., Adegoke R.M., and Aremu O.J. (2015). Potentials of Snail shell as a reinforcement for Discarded Aluminum Based Materials. *International Journal of Advanced Science and Technology*. 84, 1–8.

Arasukumar K., Basavaraju S., Bendigeri C., Umesh C.K. (2012). Studies on Mechanical Properties and Tribological Characteristics of LM25- Graphite- Silicon Carbide and LM25- Flyash- Silicon Carbide - Hybrid MMCs. *Int Journal of Innovation Research Science Engineering Technol.*1(1),107–12

Diouf S., and Molinari A.(2012). Densification mechanisms in spark plasma sintering: effect of particle size and pressure. *Powder Technol*. 221, 220–227.

Durowoju M.O., Asafa T.B., Sadiku E.R., Diouf S., Shongwe M.B., Olubambi P.A. (2019). Improving mechanical and thermal properties of graphite–aluminum composite using Si, SiC, and eggshell particles. *J Compos Mater*.

Durowoju M.O., Sadiku E.R., Diouf S., Shongwe M.B., Olubambi P.A., Mekgwe N. (2016). Effect of micron and nano-sized ZrB_2 addition on the microstructure and properties of spark plasma sintered graphite–aluminum hybrid composite. *J Mater Sci Mater Electron.* 27(5), 4672–4688.

Durowoju M.O., Sadiku E.R., Diouf S., Shongwe M.B., Olubambi P.A. (2015). Spark plasma sintering of graphite – aluminum powder reinforced with SiC / Si particles. *Powder Technol.* 284, 504–513.

Dwivedi A., and Jain M.K. (2014). Fly ash Waste Management and Overview: A Review. *Recent Res Sci Technol.* 6(1), 30–35.

Frischa M.W., Adhi Y.P., Fandi A.P., Nurul R., and Daminto. (2014). Synthesis and Characterization of Nanocrystalline Graphite from Coconut Shell with Heating Process. In: *API Conference Proceedings*. 202–206.

Fukushima H. (2009). High Thermal Conductivity Graphite-Particles-Dispersed-Composites and its Production Method. US Pat Appl Publ. 1–10.

Govindarao R., Sahoo K.L., Ganguly R.I., Dash R.R., and Narasaiah N. (2017). Effect of Flyash Treatment on the Properties of Al-6061 Alloy Reinforced with SiC–Al_2O_3–C Mixture. *Trans Indian Inst Met.* 70(10), 2707–2717.

Grabias-Blicharz E., and Franus W. (2023). A critical review on Mechano-chemical processing of fly ash and fly ash derived materials. *Science of the Total Environment*. Vol 860. 160529. doi.org/10.1016/j.scitotenv.2022.160529

Hashemi S.H. (2011). *Strength – hardness statistical correlation in API X65 steel.* 528, 1648–1655.

Huang Y., Ouyang Q., Zhang D., Zhu J., Li R., and Yu H. (2014). Carbon materials reinforced aluminum composites: A review. *Acta Metal Sin (English Letter*). 27(5), 775–786.

Kane J., Karthik C., Butt D.P., Windes W.E., and Ubic R. (2011). Microstructural Characterization and Pore structure analysis of nuclear graphite. *J Nucl Materials*. 415(2),189–97.

Karla K., Jasso A., Folliard K., Ferron R., Juenger M., and Drimalas T. (2012). Characterizing Fly Ash. 7, p172.

Karoly Z., Balazsi C., Petrik A., Labar J., and Dhar A. (2014). Hybrid aluminum matrix composites are prepared by Spark Plasma Sintering (SPS). *Eur Chem Bull*. 3(3), 247–250.

Kelechi S.E, Adamu M., Okorie A.U., Okokpujie I.P., Ibrahim Y.E., Obianyo I. I. (2022). A comprehensive review of coal fly ash and its application in the construction industry. Environmental Science Engineering. Vol 9(1). Doi:10.1080/23311916.2022.2114201

Klett J., and Conway B. (2000). Thermal management solutions utilizing high thermal conductivity graphite foams. *Int SAMPE Symp Exhib*. 45(1), 1–11.

Li D., Tian Y., and Qiao Y. (2014). Forming Active Carbon Monoliths from H3PO4-loaded Sawdust with Addition of Peanut Shell Char. *BioResources*. 9(3), 4981–4992.

McCoy J.W., and Vrable D.L. (2004). Metal Matrix Composites from Graphite Foams and Copper. *Sample Journal.* 40(1), 7–15.

Mikulionok I., (2024). A state of art and prospects of fly ash management. Energy Technologies and resources saving. Doi.10.33070/etars.3.2024.11

Priyadarshi T.R.S., and Sandhyarani B. (2014). Physical and Mechanical Behavior of Al_2O_3 Filled Jute Fiber Reinforced Epoxy Composites. *International Journal Current Engineering Technol.* (2), 67–71.

Olatinwo T.F., Woli T.O., Muhammed K.O., Orilonise A. (2024). Composites made from Natural Fiber materials: A review. ARCN International Journal of Sustainable Development, Vol 14(1), 11-23. Doi:2726-4-573-1-1412.

Rajesh K., Channabasavaraj S., Mohan N., and Mahesha C.R. (2017). Mechanical and Dry Sliding Wear behavior on fly-ash/graphite/magnesium particles reinforced aluminum (AL6061) metal matrix composites. *Int Journal of Resources Aeronaut Mech Eng*. 368–98. Available from: www.IJRAME.com

Rodriguez A., Guerrero S.S.A., Narciso J., Louis E., and Rodriguez-Reinoso F. (2006). Pressure infiltration of Al-12 wt% Si-X (X=Cu, Ti, Mg) alloys into graphite particle performs. *Acta Mater*. 54, p1821.

Rycroft M. (2017). *Exploring the many uses of fly ash*. In EE Publishers. p. 1–2. Available from: www.ee.co.za

Saheb D.A. (2011). Aluminum Silicon Carbide and Aluminum Graphite Particulates Composites. *ARPN Journal of Engineering and Applied Sciences*. 6(10), 41–46.

Selvan M.D., Sivaram N.M. (2017). Optimal Parameter Design by Taguchi method for Mechanical properties of Al6061 Hybrid Composite reinforced with Fly-ash/Graphite/Copper. *Int J ChemTech Res*. 10(13), 128–137.

Subramani N., Vijayaraghavan K., Arunsankar V.V., and Sudha K. (2013). Analysis and Investigation on A2024 Metal Matrix Composites with B_4C and Graphite. *International Journal of Innovation Res Sci Eng Technol (*An ISO Certif Organ. 2(9), 4637–4642. Available from: www.ijirset.com

Türkel S., and Aksin E. (2012). A comparative study on the use of fly ash and phosphogypsum in brick production. *Sadhana - Acad Proc Eng Sci.* 37(5), 595–607.

Viswanatha B.M., Kumar M.P., Basavarajappa S., and Kiran T.S. (2013). A356/SiC/ Gr Metal Matrix Composites. *J Eng Sci Technol.* 8(6), 754–763.

Wu X., Chen W., Wu W., Chen Y., Li T., Zhang C. (2017). Controllable preparation of large-area arrays of Al-substituted CoCuNi ferrite rods with the improvement of saturation magnetization and initial permeability. *Journal of Material Science and Ceramics*.

Yazici Ş., and Arel H.Ş. (2012). Effects of fly ash fineness on the mechanical properties of concrete. *Sadhana - Acad Proc Eng Science*. 37(3), 389–403.

Zhou C., Ji G., Chen Z., Wang M., Addad A., and Schryvers D. (2014). Fabrication, interface characterization, and modeling of oriented graphite flakes/Si/Al composites for thermal management applications. *Mater Des [Internet]*. 63(2014), 719–28. Available from: http://dx.doi.org/10.1016/j.matdes.2014.07.009.